# Journal of Materials Chemistry A

Accepted Manuscript


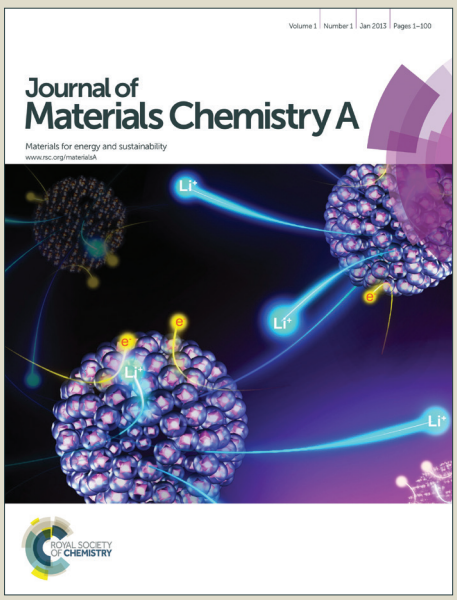





ROYAL SOCIETY OF CHEMISTRY

www.rsc.org/materialsA

Journal of Materials Chemistry A

ARTICLE

# Enhancement of hydroxide conductivity by grafting flexible pendant imidazolium groups into poly(arylene ether sulfone) as anion exchange membranes

Received 00th January 20xx,
Accepted 00th January 20xx

DOI: 10.1039/x0xx00000x

www.rsc.org/

Yi Zhi Zhuo, Ao Lan Lai, Qiu Gen Zhang, Ai Mei Zhu, Mei Ling Ye and Qing Lin Liu*

Anion exchange membranes (AEMs) have been recognized as one of the most perspective polyelectrolytes for fuel cells due to their faster electrode reaction kinetics and the potential of adopting cheaper metal catalysts against proton exchange membranes (PEMs). Herein, a series of poly(arylene ether sulfone)s containing flexible pendant imidazolium cation was synthesized by grafting bromine-bearing imidazolium-based ionic liquids into hydroxyl-bearing poly(ether sulfone) matrix. $^1$H NMR spectroscopy was used to confirm the as-synthesized copolymers. Atomic force microscopy (AFM) and small angle X-ray scattering (SAXS) were used to characterize the morphology of membranes. The incorporation of the flexible side-chain imidazolium groups is beneficial to the aggregation of the ionic clusters leading to the formation of hydrophilic/hydrophobic phase-separated morphology and nano-channels. As a result, an enhancement in the ion conductivity can be achieved. Therefore, the as-prepared AEMs possess higher ion conductivity than traditional benzyl-type AEMs. The weight-based ionic exchange capacity ($IEC_w$) of the membranes was in the range of 1.01–1.90 meq·g$^{-1}$. Correspondingly, their ion conductivity was in the range of 22.13–59.19 and 51.66–108.53 mS·cm$^{-1}$ at 30 and 80 °C, respectively. Moreover, the membranes also exhibit good alkaline stability and an interesting single cell performance. This work presents a facile and universal route for the synthesis of AEMs with superior performance.

## Introduction

Proton exchange membranes (PEMs) have been widely investigated for polymer electrolyte fuel cells (PEFCs) due to their high conductivity and high chemical stability.[1] However, the widespread commercialization of PEM-based PEFCs is impeded by their high fuel permeability and exclusive dependence on expensive Pt-based catalysts.[2,3] Anion exchange membranes (AEMs) based PEFCs, in which the charge carriers are hydroxide ions rather than protons, have received a significant interest due to their potential for surpassing those limitations. One reason is that AEM-based PEFCs operate under alkaline conditions, in which the electrode reaction kinetics will be enhanced and the catalysts are not subjected to corrosion.[4] Consequently, various cheaper metals (Ag, Co, or Ni) instead of platinum can be used as a catalyst in AEM-based PEFCs.[5,6] Furthermore, the fuel and water crossover via electro-osmotic drag may also be depressed because the transport of hydroxide ions and fuel are in the opposite directions.[7]

The advantage of AEM-based PEFCs promotes the research of AEMs. In recent years, a variety of AEMs have been prepared by the introduction of quaternary ammonium (QA),[8] imidazolium,[9] guanidinium,[10] phosphonium groups[11] or permethyl cobaltocenium[12] into various polymer backbones such as poly(styrene),[13,14] poly(vinyl alcohol),[15] poly(phenylene oxide),[16] poly(arylene ether ketone),[17] and poly(arylene ether sulfone).[18] Although a significant progress has been made on AEMs, their conductivity and alkaline stability are still required to improve for fuel cell applications.[19]

Inspired by the research of PEMs, two main methods have been proposed to improve the ion conductivity of AEMs. One is to prepare the AEMs using block copolymers,[20,21] and the other using pendant-functional-group-type (side-chain-type) polyelectrolyte.[22,23] Block copolymers used for the preparation of AEMs for fuel cells have been widely investigated because the hydrophilic/hydrophobic phase-separated structure in the designed block copolymer would lead to higher ion conductivity.[24,25] However, side-chain-type polyelectrolytes are still rarely reported for AEMs. Side-chain-type polyelectrolytes have the comb-like structure similar to that of Nafion®, and they would also form an amphiphilic phase-separated structure. Most polyelectrolyte AEMs are synthesized via chloromethylation of aromatic rings or bromination on the benzylic methyl groups of the polymers, followed by functionalization. This way can only be used to obtain benzyl-type AEMs, which cannot be considered as side-chain-type AEMs because the side chain is too short. Till now, only few researchers synthesized side-chain-type AEMs successfully. Lin and coworkers reported polyfluorene ionomer with pendant

*Department of Chemical & Biochemical Engineering, College of Chemistry & Chemical Engineering, Xiamen University, Xiamen 361005, China. E-mail: qlliu@xmu.edu.cn*

† Electronic Supplementary Information (ESI) available: $^1$H NMR spectra and the digital photo of 6BrIm; $^1$H NMR spectra of MPES-0.7, HPES-0.7 and ImPES-0.7; $^1$H NMR spectra of MPES-1.0, HPES-1.0 and ImPES-1.0; digital photo and SEM image of the ImPES-0.85 membrane. See DOI: 10.1039/x0xx00000x

imidazolium groups for alkaline fuel cell applications, however, the ionic exchange capacity is at a low level because of the bulky monomer.[26] Zhang and coworkers synthesized aromatic polyelectrolytes with pendant quaternary ammonium via polyacylation for alkaline fuel cells. Unfortunately, this approach could only lead to poly(arylene ether ketone)s polyelectrolytes.[27] Rao and coworkers reported cardo poly(arylene ether sulfone) block copolymers with pendant imidazolium side chains as novel AEMs. Nevertheless, the side part is rigid benzene ring, which will hamper the aggregation of the ionic clusters and affect the ion conductivity.[28] Hence, it is essential to design a facile and universal route to synthesize polyelectrolytes with flexible pendant functional groups for the preparation of AEMs.

Herein, we developed a facile and versatile strategy for the synthesis of a new kind of AEMs containing flexible pendant functional groups via chemical grafting reaction. Methoxy-bearing poly(ether sulfone)s (MPESs) are produced via nucleophilic substitution polycondensation, followed by demethylation to yield hydroxyl-bearing poly(ether sulfone)s (HPES). Bromine-bearing imidazolium-based ionic liquids were synthesized and grafted into poly(ether sulfone)s backbone via Williamson reaction. The synthesis and properties of the side-chain-type AEMs were investigated.

## Experimental

### Materials

1,6-Dibromohexane (98%, Aladdin, China), 1-methylimidazole (99%, Aladdin, China), methoxyhydroquinone (MHQ) (98%, J&K, China), 4,4'-(hexafluoroisopropylidene)diphenol (BPHF) (99%, Matrix, USA), bis(4-fluorophenyl) sulfone (FPS) (99.0%, TCI, Japan), boron tribromide ($BBr_3$)(99.9%, Aladdin, China), potassium iodide(99.5%, Aladdin, China) were used as received. Toluene (98.0%, Sinopharm, China) was stirred over $CaH_2$ for 24 h, then distilled under reduced pressure and stored over 4 Å molecular sieves. Acetone, chloroform ($CHCl_3$), dimethylsulfoxide (DMSO) and all other chemicals were supplied from Shanghai Sinopharm Chemical Reagent Co., Ltd (China) and used without further purification.

### Preparation of AEMs

Scheme 1 shows the synthesis of 1-(6-bromohexyl)-3-methylimidazolium bromide (6BrIm): a kind of imidazolium-based ionic liquids (ILs). An excess of 1,6-dibromohexane was fed to reduce the yield of bis-substituted by-product. The procedure for preparation of the AEMs is shown in Scheme 2. The precursor poly(ether sulfone)s containing methoxy groups (MPES-x) were synthesized via nucleophilic substitution polycondensation, followed by demethylation to yield hydroxyl-bearing poly(ether sulfone)s (HPES-x). The bromine-bearing ILs can react with HPES-x in the presence of potassium carbonate to generate imidazolium poly(ether sulfone)s (ImPES-x).

#### Synthesis of 6BrIm

6BrIm was synthesized according to a reported procedure with some modifications.[29] A mixture of 1-methylimidazole (4 mL, 4.12 g, 50 mmol) and acetone (50 mL) was placed into a 250 mL three-necked flask equipped with a magnetic stirrer, a condenser, a nitrogen inlet and outlet, and then 1,6-dibromohexane (30 mL, 48 g, 194 mmol) was added into the flask at room temperature (RT). The mixture was stirred at 40 ºC for 15 h to give a white suspension, followed by filtration to remove the white solid bis-substituted by-product. The by-product was further drained with acetone for the recovery of 6BrIm to achieve a maximum yield. The filtrate was rotor-evaporated to make a viscous pale yellow oil product by removing the acetone. The resulting product was extracted from ethyl acetate and diethyl ether several times, and dried at 50 ºC under vacuum for 24 h (yield: 75%).

#### Synthesis of MPES-x

Scheme 1 shows the synthesis of the precursor MPES-x (where x is the molar ratio of MHQ to FPS) by the nucleophilic substitution polycondensation of the as-synthesized copolymers. A typical procedure for the synthesis of MPES-0.7 is detailed as follows. FPS (10 mmol, 2.5425 g), BPAF (3mmol, 1.0087g), MHQ (7 mmol, 0.9810 g), $K_2CO_3$ (20 mmol, 2.76 g), DMAc (30 mL), and toluene (15 mL) were placed into a 100 mL three-necked flask equipped with a magnetic stirrer, a Dean-Stark trap, and a gas inlet and outlet. The reaction mixture was heated to 140 ºC to remove the azeotrope of water/toluene out of the reaction system. After 4 h, the mixture was slowly heated to 155 ºC and then stirred for 15 h. Before the end of the reaction, MHQ (0.5 mmol, 0.0710 g) was added to the reaction mixture and then the reaction was continued for another 1 h. After the reaction, the mixture was cooled to RT and poured into 400 mL of an aqueous methanol solution under vigorous stirring (methanol/deionized (DI) water=1/1, v/v) to yield a white solid precipitate. The product was washed with water and methanol for several times and dried at 80 ºC under vacuum for 24 h.

#### Synthesis of HPES-x

A typical procedure was given as follows. 2.7 g of MPES-0.7 was dissolved into 30 mL of $CHCl_3$ to make a solution in a 100 mL three-necked flask equipped with a nitrogen inlet and a mechanical stirrer. $BBr_3$ (3 mL) was mixed with $CHCl_3$ (10 mL), and then added dropwise to the MPES-0.7 solution at 0 ºC to take a reaction. After 6 h, the resulting powder (HPES-0.7) was filtered, washed with $CHCl_3$ and water for several times and dried at 60 ºC for 24 h.

#### Synthesis of ImPES-x

HPES-0.7 (2.0 g), $K_2CO_3$ (1.38 g, 10 mmol), KI (0.083g, 0.5mmol), and DMSO (30 mL) were mixed in a 100 mL three-necked flask equipped with a magnetic stirrer, a nitrogen inlet and outlet. The mixture was then heated to 100 ºC to dissolve

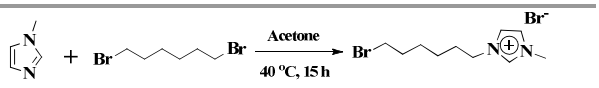


**Scheme 1** Synthesis of 1-(6-bromohexyl)-3-methylimidazolium bromide (6BrIm).

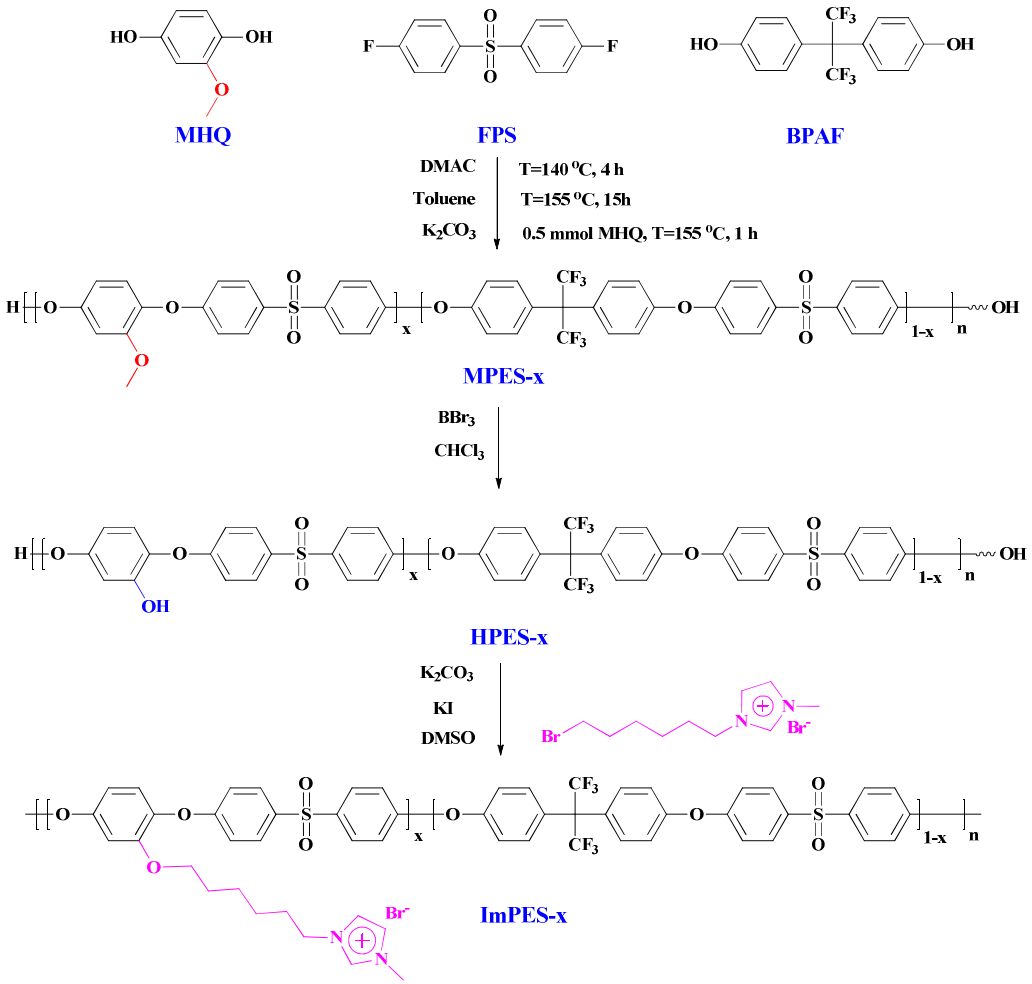


**Scheme 2** Synthesis of the methoxy-bearing poly(ether sulfone)s (MPES), hydroxyl-bearing poly(ether sulfone)s (HPES) and imidazolium poly(ether sulfone)s (ImPES).

HPES-0.7 completely. 6BrIm (2.6320 g, 8 mmol) was added to the mixture and stirred at 100 ºC for 12 h. After the reaction, the mixture was cooled to RT and poured into 200 mL of acetone to form a taupe solid precipitate (ImPES-0.7), then washed with acetone and DI water for several times.

### Membrane fabrication and alkalization

The ImPES-x was dissolved in DMSO (3% w/v), followed by filtration through a 0.45 μm PTFE syringe filter to make a transparent yellowish-brown solution. The resulting solution was cast onto a clean glass plate, followed by drying at 60 ºC under vacuum for 24 h to form a film. The obtained film was peeled off and then soaked in a 1.0 M aqueous potassium hydroxide solution at RT for 48 h, followed by washing with DI water several times and immersing in DI water at least for 48 h before evaluation.

## Structure characterization

$^1$H NMR spectra were recorded on Avancell 500 MHz (Bruker, Switzerland) using dimethyl sulfoxide-d6 (DMSO-d6) as the solvent and tetramethylsilane (TMS) as the standard. The mechanical properties of the membranes ($OH^-$ type) were measured using a universal tester (WDW-1E Testing System) with a crosshead speed of 5 mm·min$^{-1}$ at RT. The thermal stability was evaluated on a thermogravimetric analyzer (SDT-Q600, TA, USA) from RT to 800 °C at a heating rate of 10 °C·min$^{-1}$ under a nitrogen atmosphere. A field emission scanning electron microscope (SEM, Zeiss Sigma, Germany) was used to characterize the morphology of the membranes. The surface micrograph of the AEMs was observed via an atomic force microscope (AFM) (5500, Agilent Technologies). Tapping mode was used in the observation under ambient condition (25 ºC, 60% relative humidity (RH)). Small angle X-ray scattering (SAXS) profiles of the AEMs were recorded using a SAXSess-MC2 X-ray scattering spectrometer (Anton Paar, Austria) at RT.

## Characterization of AEMs

### Ion conductivity

The resistance (R) of the membrane samples ($OH^-$ type) was measured over the frequency range from 100 mHz to 100 kHz by the two-electrode AC impedance spectroscopy method using

a Parstat 263 electrochemical workstation (Princeton Advanced Technology, USA). All of the samples were tested in a $N_2$-protected chamber with DI water. The ion conductivity, σ ($S \cdot cm^{-1}$), is calculated as follows

$$\sigma = \frac{l}{AR} \quad (1)$$

where $l$ (cm) is the distance between the two copper electrodes, and $A$ ($cm^2$) is the cross-sectional area of the tested membrane.

### Water uptake (WU)

The *WU* was examined using a quartz spring balance as previously reported.[30] The *WU* of the membrane ($OH^-$ type) can be calculated by Hooke's law

$$WU = \frac{kL_3 - kL_2}{kL_2 - kL_1} \times 100\% = \frac{L_3 - L_2}{L_2 - L_1} \times 100\% \quad (2)$$

where $k$ is the elasticity coefficient of the quartz spring, and $L_1$, $L_2$ and $L_3$ are the length of the quartz spring without loading, loaded with the dry and the wet membranes, respectively.

### Swelling ratio (SR)

The change in the length of the membrane ($OH^-$ type) before and after being immersed in water at a given temperature for 24 h can be used to estimate the *SR* of the membrane:

$$SR = \frac{(L_w \times W_w)^{1/2} - (L_d \times W_d)^{1/2}}{(L_d \times W_d)^{1/2}} \times 100\% \quad (3)$$

where $L_d$ and $W_d$ are the length and the width of the dry membrane, respectively, and $L_w$ and $W_w$ are the length and the width of the wet membrane, respectively.

### Ionic exchange capacity (IEC)

The weight-based *IEC* ($IEC_w$, $meq \cdot g^{-1}$) is calculated by:

$$IEC_w = \frac{1000x}{xW_x + (1-x)W_{1-x}} \quad (4)$$

where $x$ is the molar ratio of MHQ to FPS, and $W_x$ (525.64 $g \cdot mol^{-1}$) and $W_{1-x}$ (550.47 $g \cdot mol^{-1}$) are the molecular weights of the ionized repeating unit ($OH^-$ type) and the unionized repeating unit, respectively.

The $IEC_w$ is measured by $^1$H NMR spectra and the standard back-titration method as reported previously.[31]

The volume-based *IEC* value ($IEC_v$, $meq \cdot cm^{-3}$) can be calculated by:

$$IEC_{v,dry} = \rho \times IEC_w, \quad IEC_{v,wet} = \frac{IEC_{v,dry}}{1 + WU} \quad (5)$$

where $\rho$ ($g \cdot cm^{-3}$) is the density of the membrane, and $IEC_{v,dry}$ and $IEC_{v,wet}$ are the $IEC_v$ of the dry and the wet membranes, respectively.

### Alkaline stability

The alkaline stability of the AEMs was evaluated by monitoring the variation of IEC and conductivity after the membrane was immersed in a 2M KOH solution at 60 and 80 ºC for different time from 24 to 504 h.

### Membrane electrode assembly (MEA) and single cell performance

The carbon paper loaded with 1 $mg \cdot cm^{-2}$ Pt (Johnson Matthey) was used for the anode and cathode electrodes. The electrodes were painted with an ImPES-0.85 solution (5% w/v, DMSO), the ImPES-0.85 membrane was then sandwiched between the two electrodes with the catalyst layer facing the membrane, followed by hot-pressing at 70 ºC for 2 min. The feed of $H_2$ on the anode and $O_2$ on the cathode was at the rate of 50 and 100 $mL \cdot min^{-1}$, respectively. Single cell performance was evaluated at 60 °C with a RH of 100% using an electronic load (ZY8714, ZHONGYING Electronic Co., Ltd.).

## Results and Discussion

### Synthesis and characterization of ILs and polymers

6BrIm was synthesized via the nucleophilic substitution reaction of 1,6-dibromohexane with 1-methylimidazole (Scheme 1). An excess of 1,6-dibromohexane was used to depress the yield of bis-substituted by-product. The structure of 6BrIm was identified by $^1$H NMR in DMSO-d6. As shown in Fig. S1†, the peaks at 9.27, 7.83 and 7.75 ppm are assignable to the imidazolium groups and the resonance at 3.87 ppm is attributed to the methyl on imidazolium group. The peaks at 4.19, 3.53, 1.80, 1.41 and 1.27 ppm are ascribed to the methylene of the aliphatic chain. All of the peaks are well-assigned and confirm the structure of 6BrIm.

Methoxy-bearing poly (ether sulfone)s with different molar percentages of methoxy groups were synthesized at various feed molar ratios of MHQ to FPS (0.55, 0.7, 0.85 and 1.0) via poly-condensation (Scheme 2). Fig. S2(a)† shows the $^1$H NMR spectrum of MPES-0.7 as a typical example. All of the aromatic protons are assigned to the proposed copolymer structure. In the aromatic region, the peaks around 6.73 and 7.40 ppm are associated with the protons on the benzene ring (4 and 7 in Fig. S2(a)†). The real ratio of MHQ to FPS ($x$) can be calculated by $x = S_4/(S_7/4+S_4)$, where $S_4$ and $S_7$ are the integrals of peaks 4 and 7, respectively. The $^1$H NMR spectrum of MPES-0.7 gives $x$=0.69. The peak around 3.67 ppm (a in Fig. S2(a)†) is associated with the methoxy group.

Hydroxyl-bearing poly(ether sulfone)s were synthesized from the methoxy-bearing poly(ether sulfone)s via demethylation. The $^1$H NMR spectrum in Fig. S2† illustrates a full conversion of MPES-0.7 to HPES-0.7. After demethylation of MPES-0.7, a new peak around 10.11 ppm assignable to the phenolic hydroxyl group (b in Fig. S2(b)†) is observed, while the resonance for the methoxy group disappeared.

**Table 1** Mechanical properties of the AEMs.

| Membrane | Tensile strength (MPa) | Young's modulus (MPa) | Elongation at break (%) |
|---|---|---|---|
| ImPES-0.55 | 44.60 | 608 | 8.83 |
| ImPES-0.7 | 34.40 | 475 | 8.90 |
| ImPES-0.85 | 29.88 | 195 | 10.60 |
| ImPES-1.0 | 26.72 | 175 | 13.73 |

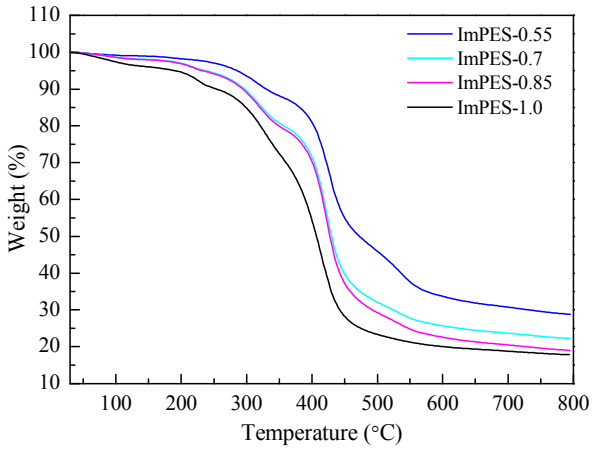


**Fig. 1** TGA curves of the ImPES-x membranes under a nitrogen flow. Heating rate: 10 °C/min.

Imidazolium poly (ether sulfone)s were synthesized from the hydroxyl-bearing poly(ether sulfone)s and bromine-bearing ILs via Williamson reaction. The reaction was conducted using potassium carbonate and potassium iodide as the catalyst. Fig.S2(c)† shows the $^{1}$H NMR spectrum of ImPES-0.7. The characteristic peaks of the methylene protons of the imidazolium ring at 9.12 ppm (i in Fig. S2(c)†) and 7.71–7.73 ppm (j and k in Fig. S2(c)†), the methyl protons at 3.85 ppm (l in Fig. S2(c)†) and the methylene protons of the aliphatic chain at around 3.89–4.08 ppm (c and h in Fig. S2(c)†) and 1.05–1.61 ppm (d, e, f and g in Fig. S2(c)†) indicate the successful introduction of the imidazolium groups into the AEMs.

Exceptionally, MPES-1.0 contains only the MHQ segment. Therefore, MPES-1.0 does not show any characteristic resonance (Fig. S3†) of the BPHF which can be observed from MPES-0.7 (the chemical shifts of 6 and 7 in Fig. S2†).Other well-assigned peaks indicate the successful synthesis of MPES-1.0, HPES-1.0 and ImPES-1.0.

### Mechanical properties and thermal stability

AEMs must possess sufficient mechanical strength for fuel cell applications. The mechanical properties of the AEMs are listed in Table 1. The ImPES-x membranes had tensile strength at break in the range of 26.72–44.60 MPa, Young's modulus of 175–608 MPa and tensile elongations at break of 8.83–13.73% at RT with 60% RH. The tensile strength of the ImPES-x membranes decreased with increasing IEC. The elongations at break of the AEMs increased with increasing IEC. This is probably due to that the higher hydrophilic segment ratio results in a higher water content and swelling of the membranes. The water can serve as a plasticizer to depress the mechanical properties of the membranes.[32]

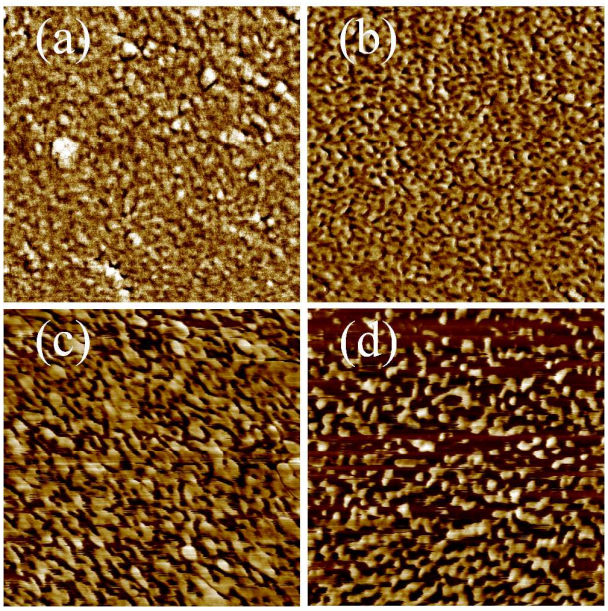


**Fig. 2** AFM phase image of (a) ImPES-0.55, (b) ImPES-0.7, (c) ImPES-0.85 and (d) ImPES-1.0 membranes. Scale: 500×500 nm

The thermal gravimetric analysis (TGA) of the ImPES-x membranes was performed from RT to 750 ºC with a heating rate of 10 ºC/min under a nitrogen flow. The first stage of weight loss below 130 ºC can be attributed to the evaporation of the residual solvent and water (Fig. 1). The second stage starting from 210 ºC is due to the degradation of imidazolium groups. The third stage from ~280 ºC results from the degradation of aliphatic side chain. The main-chain decomposition takes place above 400 ºC. The TGA curves demonstrate that the as-prepared AEMs have good thermal stability below 200 ºC, and can be used in AEMFCs.

### Membrane morphology

Fig. S4† shows the digital photos and SEM images of the ImPES-0.85 membrane. The membrane is found to be transparent, tough and flexible from Fig. S4(a) & (b)†. Furthermore, a smooth, homogeneous and defect-free surface can be observed from Fig. S4(c)†. The thickness of the membrane is about 23 μm, as shown in Fig. S4(d)†.

The phase image of the AEMs was examined by AFM in a tapping mode to address the hydrophilic/hydrophobic phase-separation.[27,28] As shown in Fig. 2, the phase image of the ImPES-x membranes was recorded on the size scale of 500×500 nm$^2$ under ambient condition. The darker region corresponds to the soft hydrophilic domain mainly consisting of water and imidazolium ionic clusters, and the brighter region corresponds to the hard hydrophobic matrix which was probably made up of aromatic polymer backbones. The size of the ionic domains and the degree of hydrophilic/hydrophobic phase-separation increase with increasing side-chain segment ratio, as clearly observed in Fig. 2. All of the ImPES-x membranes show well-defined phase separation. Especially, the ionic domains of ImPES-0.85 and ImPES-1.0 assembled into more pronounced and inter-connected nano-channels.

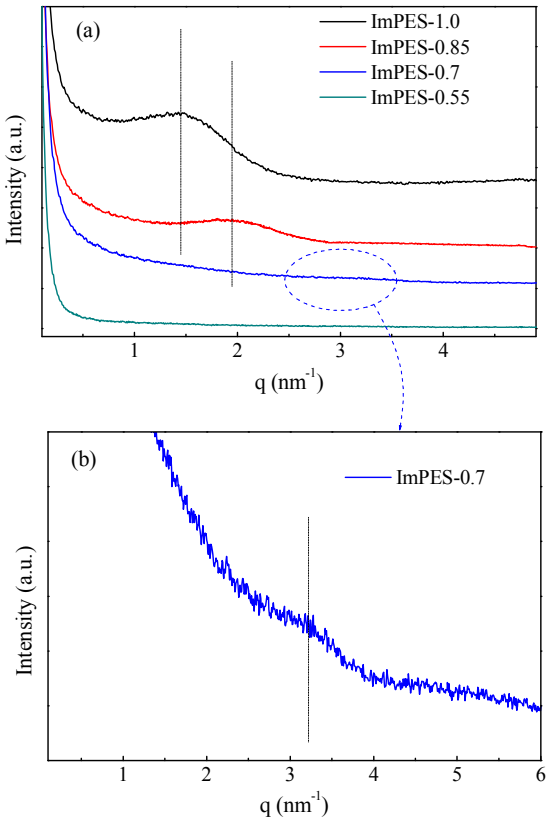


**Fig. 3** SAXS profiles of (a) the AEMs and (b) ImPES-0.7 in a high magnification.

Furthermore, SAXS was used to examine the microphase-separation of AEMs. The SAXS profiles of the ImPES-x membranes are shown in Fig. 3. The ImPES-x membrane with higher side-chain segment ratio showed higher scattering peak, which is indicative of the spacing of ion conducting channels.[33] As shown in Fig. 3(a), ImPES-1.0 and ImPES-0.85 have scattering peaks at 1.44 and 1.95 $nm^{-1}$, respectively. We can also observe the scattering peak of ImPES-0.7 at 3.20 $nm^{-1}$ from the magnified SAXS profile (Fig. 3(b)). However, no obvious peak was observed for the ImPES-0.55 membrane because the interdomain spacing is too small. The average interdomain spacing, d, of the membranes can be obtained from Bragg equation ($d=2\pi/q$). ImPES-1.0, ImPES-0.85 and ImPES-0.7 have an average interdomain spacing of 4.36, 3.22 and 1.96 nm, respectively. The Bragg spacing increased with increasing the side-chain segment ratio. This result is confirmed by the AFM observation. The reason may be that the AEMs with higher imidazolium group ratio tend to aggregate easily to form larger ionic domains.

### IEC, water uptake (WU) and swelling ratio (SR)

As a basic parameter, IEC plays a key role in the water uptake and conductivity of an ion exchange membrane. The IEC of the ImPES-x membranes is listed in Table 2. Theoretical values are calculated from the feed monomer ratio. Experimental values are determined by $^1$H NMR with the assumption that all the methoxy groups are converted to hydroxyl groups which are all grafted onto the ILs. The experimental values of $IEC_w$

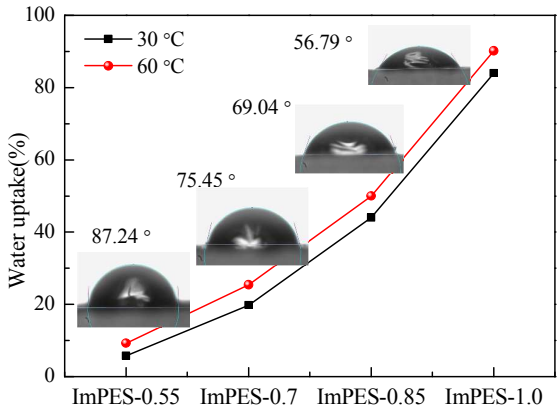


**Fig. 4** Water uptake and static water contact angle of the ImPES-x membranes.

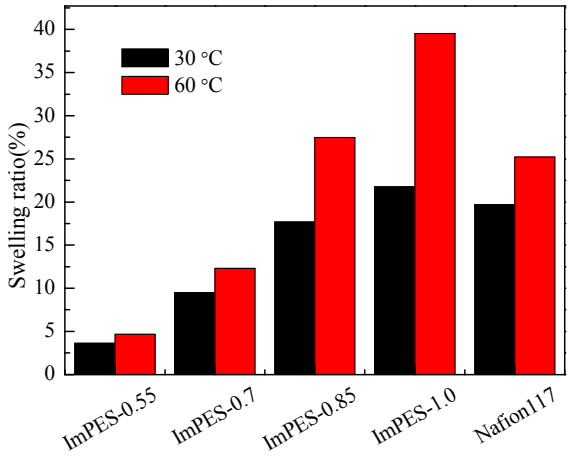


**Fig. 5** Swelling ratio of the ImPES-x membranes and Nafion® 117.

(determined by $^1$H NMR) in the range of 1.01–1.90 meq·$g^{-1}$ are close to the theoretical ones. The titrated $IEC_w$ of the as-prepared AEMs agreed well with that from $^1$H NMR, demonstrating that $Br^-$ was mostly replaced by $OH^-$.

Table 2 lists the water uptake (WU) of the ImPES-x membranes at 30 and 60 ºC. As expected, WU increased with increasing gravimetric $IEC_w$ and temperature. Fig. 4 shows the water uptake and the static water contact angle of the AEMs. The static water contact angle of the ImPES-x membranes decreased from 87.24 ° to 56.79 ° with increasing $IEC_w$. The AEM with higher $IEC_w$ tends to be more hydrophilic resulting in higher water uptake.

Table 2 shows the swelling ratio (SR) of the ImPES-x membranes at 30 and 60 ºC. The swelling ratio agrees with the WU. The SR of the ImPES-x membranes at various temperatures is shown in Fig. 5 against Nafion® 117. ImPES-0.85 has a similar SR with Nafion® 117. Therefore, ImPES-0.85 may possess promising dimension stability for fuel cells. ImPES-1.0 shows the highest SR of 21.75 at 30 ºC and 39.55 at 60 ºC.

The $IEC_v$ (wet) reflects the ion content within the ion exchange membrane under hydrated condition, without distinguishing between those ions that are mostly associated

**Table 2** IEC, density, water uptake and swelling ratio of the AEMs.

| Membrane | x [a] | $IEC_w$ (meq·g$^{-1}$) The. [b] | $IEC_w$ (meq·g$^{-1}$) Exp. [a] | $IEC_w$ (meq·g$^{-1}$) Exp. [c] | Density (g·cm$^{-3}$) | $IEC_v$ (meq·cm$^{-3}$) Dry | $IEC_v$ (meq·cm$^{-3}$) Wet [d] | WU (%) 30 °C | WU (%) 60 °C | SR (%) 30 °C | SR (%) 60 °C |
|---|---|---|---|---|---|---|---|---|---|---|---|
| ImPES-0.55 | 0.54 | 1.02 | 1.01 | 0.98 | 1.34 | 1.36 | 1.29 | 5.73 | 9.25 | 3.63 | 4.66 |
| ImPES-0.7 | 0.69 | 1.31 | 1.29 | 1.23 | 1.37 | 1.77 | 1.48 | 19.77 | 25.42 | 9.49 | 12.30 |
| ImPES-0.85 | 0.84 | 1.61 | 1.58 | 1.52 | 1.39 | 2.20 | 1.53 | 43.98 | 50.00 | 17.67 | 27.46 |
| ImPES-1.0 | 1.00 | 1.90 | 1.90 | 1.83 | 1.45 | 2.76 | 1.50 | 83.95 | 90.12 | 21.75 | 39.55 |

[a] Experimental values, determined by $^1$H NMR. [b] Theoretical values, calculated from the feed monomer ratio. [c] Experimental values, determined by back-titration. [d] Determined at 30 °C.

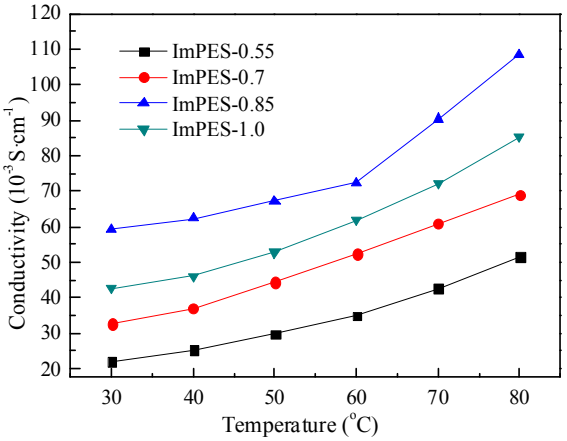


**Fig. 6** Temperature dependence of ion conductivity of the AEMs.

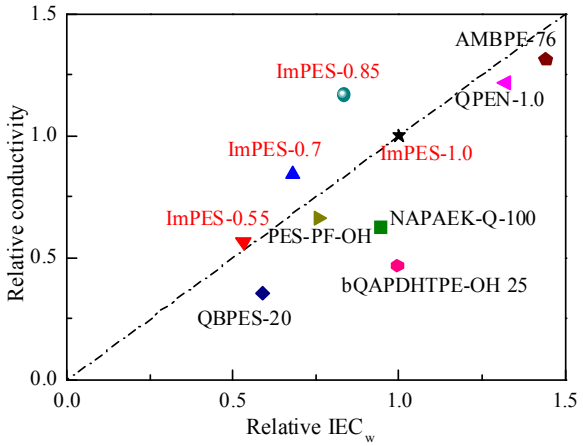


**Fig. 7** Relative conductivity as a function of relative $IEC_w$ of the ImPES-x, AMBPE-76, QPEN-1.0, PES-PF-OH, NAPAEK-Q-100, bQAPDHTPE-OH 25 and QBPES-20 at 60 °C.

with the imidazolium groups and those that are fully dissociated.[34] As listed in Table 2, the $IEC_v$ (wet) of the ImPES-x membranes increased from 1.29 to 1.53 meq·cm$^{-3}$ corresponding to an increase in $IEC_w$ from 1.01 to 1.90 meq·g$^{-1}$. However, ImPES-0.85 has a higher $IEC_v$ (wet) than ImPES-1.0, because the latter has an excess of water uptake leading to a higher swelling of the membranes and dilution of the ions after equilibrated with water.

### Hydroxide conductivity

The ion conductivity of the membrane is of particular significance and plays an important role in the performance of AEMFCs. High ion conductivity results in a high power density. Fig. 6 shows the conductivity of the ImPES-x membranes at different temperatures. All the membranes exhibited high conductivity above the magnitude of $10^{-2}$ S·cm$^{-1}$ over the temperature range. The ion conductivity of the membranes steadily increased with increasing temperature because of the enhanced water diffusion and ion migration. Normally, the increment in conductivity is pertinent to the increase in $IEC_w$. Interestingly, with an amphiphilic structure ImPES-0.85 has higher ion conductivity than ImPES-1.0. ImPES-0.85 shows a conductivity of 59.19 mS·cm$^{-1}$ at 30 ºC and 108.53 mS·cm$^{-1}$ at 80 ºC. ImPES-1.0 shows the value of 42.70 and 85.30 mS·cm$^{-1}$ at 30 and 80 ºC, respectively. This can be attributed to excessive water absorption of ImPES-1.0 leading to a lower $IEC_v$ of ImPES-1.0 than ImPES-0.85. The main reason for such high ion conductivity is that the incorporation of flexible side-chain imidazolium groups could be beneficial to the aggregation of the ionic clusters. This subsequently leads to the formation of hydrophilic/hydrophobic phase-separated morphology (as confirmed by AFM) and nano-channels to enhance the ion conductivity.[34,35] As shown above, the membranes with longer hydrophilic segments exhibited larger and more developed interconnected ion-conducting channel, which should normally be favorable for higher conductivity. However, the hydrophilic domain of ImPES-1.0 is too large resulting in excessive water absorption and thus a negative effect on ion conductivity.

We introduced relative conductivity as a function of relative $IEC_w$ to demonstrate the side-chain-type AEMs having higher ion conductivity than benzyl-type AEMs, as shown in Fig. 7. The ImPES-1.0 membrane is used as the basis for comparison. We set both the conductivity and $IEC_w$ of ImPES-1.0 to be 1. The conductivity and $IEC_w$ of other AEMs are divided by those of ImPES-1.0 to get the relative conductivity and relative $IEC_w$, respectively. It should be noted that IEC usually dominates ion conductivity with almost a linear relationship. Hence, it is more practical to assess the intrinsic hydroxide conduction of AEMs from Fig. 7. Target membranes with high ion conductivity are ideally located in the upper left-hand corner (Fig. 7). The as-prepared membranes are located in this target area. One thus concludes that the ion conductivity of the ImPES-x membranes is higher than most random copolymer AEMs (QPEN-1.0,[36] PES-PF-OH,[37] NAPAEK-Q-100[38]), and even higher than some block copolymer AEMs (AMBPE-76,[39] bQAPDHTPE-OH 25,[40] QBPES-20[41]). This definitely demonstrates that the incorporation of long side-chain imidazolium groups could enhance the hydroxide conductivity.

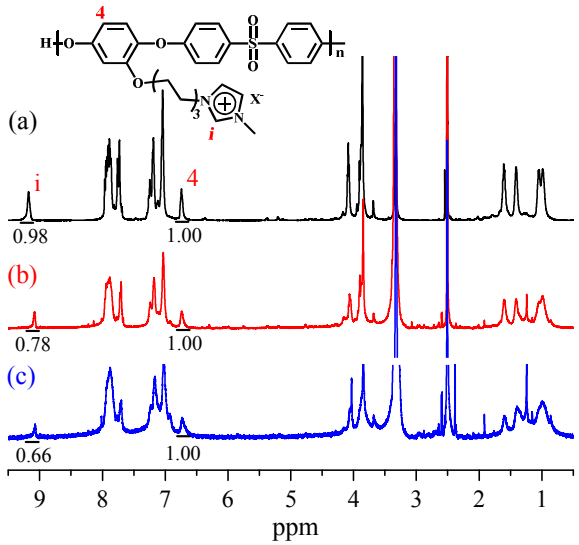


**Fig. 8** $^{1}$H NMR spectra of ImPES-1.0: (a) original $Br^{-}$ type sample, (b) after immersion in a 2M KOH solution at 60 °C for 504 h and (c) after immersion in a 2M KOH solution at 80 °C for 504 h.

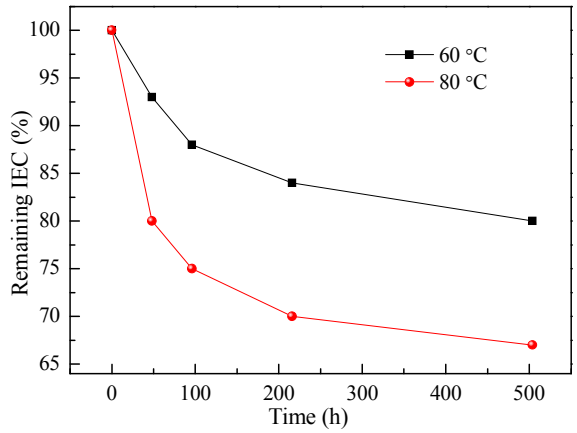


**Fig. 9** Remaining IEC of ImPES-1.0 in a 2M KOH solution at 60 and 80 °C.

**Table 3** $IEC_w$ and conductivity of ImPES-1.0 before and after immersion in a 2M KOH solution for 504 h.

| | $IEC_w$ [a] (meq·g$^{-1}$) | | Conductivity [b] (mS·cm$^{-1}$) | |
|---|---|---|---|---|
| Temperature (°C) | Before | after | Before | after |
| 60 | 1.83 | 1.39 | 42.70 | 30.29 |
| 80 | 1.83 | 1.17 | 42.70 | 24.35 |

[a] determined by back-titration. [b] measured at 30 °C.

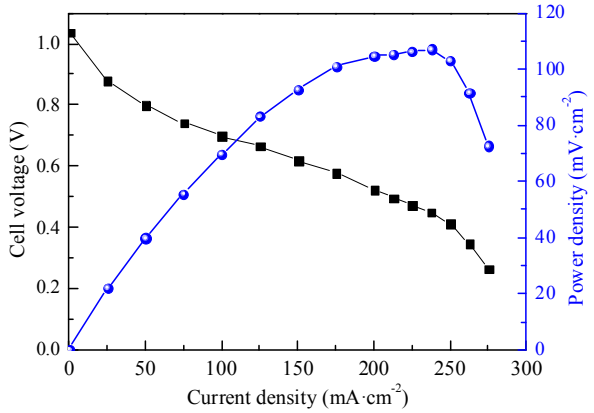


**Fig. 10** Polarization curve of a single cell using ImPES-0.85 with air at ambient pressure (60 °C, 100% RH)

### Alkaline stability

The alkaline stability of AEMs is one of the vital problems and should be considered for practical application. Traditionally, the alkaline stability of AEMs was investigated by monitoring the variation of conductivity and IEC via titration after accelerated tests. However, some limitations still exist in these methods. The variation of conductivity might not reflect the deformation of the chemical structure of AEMs and there is some uncertainty in determining IEC via titration. Here, we evaluated the alkaline stability of ImPES-1.0 by immersing the membrane in a 2 M KOH solution at 60 ºC and 80 ºC. The change in the chemical structure of ImPES-1.0 was characterized by $^{1}$H NMR spectra. Fig. 8 shows the $^{1}$H NMR spectra of ImPES-1.0 before and after alkaline stability test at different conditions. Compared with Fig. S2(c)†, all peaks in Fig. 8 are well-assigned. Peak 4 is ascribed to the protons on the backbone benzene ring and peak i is assigned to the imidazolium group. The remaining IEC can be obtained by dividing the integral of peak i of the sample before test by that of the sample after accelerated test. After immersion in a 2 M KOH solution at 60 ºC for 504 h, about 80% the imidazolium group is left. Even after immersion in a 2 M KOH solution at 80 ºC for 504 h, there is still about 67% the imidazolium group could retain. The change of remaining IEC in test conditions is shown in Fig. 9. At the beginning, the remaining IEC of the ImPES-1.0 membrane drops rapidly, and then becomes mild. The decline is ascribed to the degradation of imidazolium groups by the attack of hydroxide ions. Moreover, $IEC_w$ (determined by back-titration) and conductivity (measured at 30 °C) of ImPES-1.0 before and after immersion in a 2M KOH solution for 504 h are shown in Table 3. The conductivity of the ImPES-1.0 membrane decreased from 1.83 to 1.39 meq·cm$^{-3}$ and was accompanied by a decrease in $IEC_w$ from 42.70 to 30.29 mS·cm$^{-1}$ after immersion in a 2M KOH solution at 60 °C for 504 h. After immersion in a 2M KOH solution at 80 °C for 504 h, the $IEC_w$ of the ImPES-1.0 membrane dropped to 1.17 meq·cm$^{-3}$, and the conductivity dropped to 24.35 mS·cm$^{-1}$. In summary, ImPES-1.0 exhibited a good alkaline stability probably resulting from the presence of the five-membered heterocyclic ring.[42,43] Furthermore, the hydrophilic/hydrophobic phase-separated structure, as confirmed by AFM, may be favorable to the alkaline stability of AEMs. The reason is that $OH^{-}$ can be well-solvated in a hydrophilic micro-environment, and the better solvation of $OH^{-}$ may lead to a slower chemical reaction of the functional groups.[27,44] Furthermore, according to the report,[45] polyelectrolytes with long alkylene or alkyleneoxymethylene spacers (at least four carbon atoms) between the benzene ring and the functional head-group exhibited much higher alkaline stability than commercial ones with the –CH2– spacer. However, there's still some room for improvement in the alkaline stability. Many reports revealed that C2-substituted imidazolium cation shows better alkaline stability than C2-unsubstituted imidazolium cation due to the

steric hindrance.[46-51] This inspires us to improve the alkaline stability in the future.

### Single cell performance

The performance of a single cell using ImPES-0.85 was examined with air at 60 ºC and ambient pressure with 100% RH. The polarization and power density-current density relationship curves are shown in Fig. 10. The open circuit voltage (OCV) of the as-fabricated single cell was 1.037 V, indicating that the membrane had a good gas barrier property. A maximum power density of 107.2 $mW \cdot cm^{-2}$ can be achieved at a current density of 237.5 $mA \cdot cm^{-2}$. Without optimization, the peak power density already reached to a promising level. Further work will focus on the optimization of the MEA construction and the operational conditions.

## Conclusions

In summary, flexible pendant imidazolium cation is successfully tethered to poly(arylene ether sulfone) via Williamson reaction in a mild condition. A comparison with traditional benzyl-type AEMs shows that the AEMs containing flexible side chain pendant with imidazolium cations exhibit higher ion conductivity. This is probably due to the formation of inter-connected nano-channels resulting from the well-defined hydrophobic/hydrophilic phase-separated structure. In addition, the structure is also favorable to the alkaline stability of the as-prepared AEMs. And the water uptake of the ImPES-x membranes varied in the range 5.73%–83.95% at 30 ºC and 9.25%–90.12% at 60 ºC. Meanwhile, the swelling ratio is in the range 3.63%–21.75% at 30 ºC and 4.66%–39.55% at 60 ºC. Furthermore, the membranes also show good thermal stability and mechanical properties. The facile route for synthesizing polymer containing flexible pendant imidazolium groups as AEMs may be suitable for other polymer matrixes.

## Acknowledgment

Financial support from the National Nature Science Foundation of China (grant no. 21376194), the Nature Science Foundation of Fujian Province of China (grant no. 2014H0043), and the research fund for the Priority Areas of Development in Doctoral Program of Higher Education (no. 20130121130006) is gratefully acknowledged.

## Notes and references

1 K. A. Mauritz and R. B. Moore, *Chem. Rev.*, 2004, **104**, 4535-4586.
2 R. Bashyam and P. Zelenay, *Nature*, 2006, **443**, 63-66.
3 M. Tanaka, K. Fukasawa, E. Nishino, S. Yamaguchi, K. Yamada, H. Tanaka, B. Bae, K. Miyatake and M. Watanabe, *J. Am. Chem. Soc.*, 2011, **133**, 10646-10654.
4 N. Li, Y. Leng, M. A. Hickner and C. Y. Wang, *J. Am. Chem. Soc.*, 2013, **135**, 10124-10133.
5 G. Merle, M. Wessling and K. Nijmeijer, *J. Membr. Sci.*, 2011, **377**, 1-35.
6 S. Gu, W. Sheng, R. Cai, S. M. Alia, S. Song, K. O. Jensen and Y. Yan, *Chem. Commun.*, 2013, **49**, 131-133.
7 S. C. Price, X. Ren, A. C. Jackson, Y. Ye, Y. A. Elabd and F. L. Beyer, *Macromolecules*, 2013, **46**, 7332-7340.
8 J. Yan and M. A. Hickner, *Macromolecules*, 2010, **43**, 2349-2356.
9 F. Zhang, H. Zhang and C. Qu, *J. Mater. Chem.*, 2011, **21**, 12744-12752.
10 D. S. Kim, A. Labouriau, M. D. Guiver and Y. S. Kim, *Chem. Mater.*, 2011, **23**, 3795-3797.
11 S. Gu, R. Cai, T. Luo, Z. Chen, M. Sun, Y. Liu, G. He and Y. Yan, *Angew. Chem. Int. Ed.*, 2009, **48**, 6499-6502.
12 S. Gu, J. Wang, R. B. Kaspar, Q. Fang, B. Zhang, E. B. Coughlin and Y. Yan, *Sci. Rep*., 2015, **5**, 11668.
13 Q. H. Zeng, Q. L. Liu, I. Broadwell, A. M. Zhu, Y. Xiong and X. P. Tu, *J. Membr. Sci.*, 2010, **349**, 237-243.
14 J. R. Varcoe, R. C. T. Slade, E. L. H. Yee, S. D. Poynton and D. J. Driscoll, *J. Power Sources*, 2007, **173**, 194-199.
15 Y. Xiong, J. Fang, Q. H. Zeng and Q. L. Liu, *J. Membr. Sci.*, 2008, **311**, 319-325.
16 J. Ran, L. Wu, J. R. Varcoe, A. L. Ong, S. D. Poynton and T. Xu, *J. Membr. Sci.*, 2012, **415**, 242-249.
17 A. Jasti, S. Prakash and V. K. Shahi, *J. Membr. Sci.*, 2013, **428**, 470-479.
18 J. Pan, S. Lu, Y. Li, A. Huang, L. Zhuang and J. Lu, *Adv. Funct. Mater.*, 2010, **20**, 312-319.
19 J. R. Varcoe, P. Atanassov, D. R. Dekel, A. M. Herring, M. A. Hickner, P. A. Kohl, A. R. Kucernak, W. E. Mustain, K. Nijmeijer, K. Scott, T. Xu and L. Zhuang, *Energy Environ. Sci.*, 2014, **7**, 3135-3191.
20 B. Bae, K. Miyatake and M. Watanabe, *Macromolecules*, 2010, **43**, 2684-2691.
21 A. S. Badami, O. Lane, H. S. Lee, A. Roy and J. E. McGrath, *J. Membr. Sci.*, 2009, **333**, 1-11.
22 T. B. Norsten, M. D. Guiver, J. Murphy, T. Astill, T. Navessin, S. Holdcroft, B. L. Frankamp, V. M. Rotello and J. Ding, *Adv. Funct. Mater.*, 2006, **16**, 1814-1822.
23 B. Lafitte and P. Jannasch, *Adv. Funct. Mater.*, 2007, **17**, 2823-2834.
24 N. Yokota, H. Ono, J. Miyake, E. Nishino, K. Asazawa, M. Watanabe and K. Miyatake, *ACS Appl. Mater. Interfaces*, 2014, **6**, 17044-17052.
25 M. L. Disabb-Miller, Z. D. Johnson and M. A. Hickner, *Macromolecules*, 2013, **46**, 949-956.
26 B. Lin, L. Qiu, B. Qiu, Y. Peng and F. Yan, *Macromolecules*, 2011, **44**, 9642-9649.
27 Z. Zhang, L. Wu, J. Varcoe, C. Li, A. L. Ong, S. Poyoton and T. Xu, *J. Mater. Chem. A*, 2013, **1**, 2595-2601.
28 A. H. N. Rao, H. J. Kim, S. Nam and T. H. Kim, *Polymer*, 2013, **54**, 6918-6928.
29 A. Pertegás, N. M. Shavaleev, D. Tordera, E. Ortí, M. K. Nazeeruddin and H. J. Bolink, *J. Mater. Chem. C*, 2014, **2**, 1605-1611.
30 P. Y. Xu, K. Zhou, G. L. Han, Q. G. Zhang, A. M. Zhu and Q. L. Liu, *ACS Appl. Mater. Interfaces*, 2014, **6**, 6776-6785.
31 A. N. Lai, L. S. Wang, C. X. Lin, Y. Z. Zhuo, Q. G. Zhang, A. M. Zhu and Q. L. Liu, *ACS Appl. Mater. Interfaces*, 2015, **7**, 8284-8292.
32 H. N. Dhakal, Z. Y. Zhang and M. O. W. Richardson, *Compos. Sci. Technol*., 2007, **67**, 1674-1683.
33 K. D. Kreuer, S. J. Paddison, E. Spohr and M. Schuster, *Chem. Rev.*, 2004, **104**, 4637-4678.
34 C. Wang, N. Li, D.W. Shin, S. Y. Lee, N. R. Kang, Y. M. Lee and M. D. Guiver, *Macromolecules*, 2011, **44**, 7296-7306.
35 L. Zhang, G. Zhang, C. Zhao, Z. Liu, H. Jiang, S. Xu, M. Li, D. Xu and H. Na, *Int. J. Hydrogen Energy*, 2013, **38**, 12363-12373.

36 A. N. Lai, L. S. Wang, C. X. Lin, Y. Z. Zhuo, Q. G. Zhang, A. M. Zhu and Q. L. Liu, *J. Membr. Sci.*, 2015, **481**, 9-18.
37 Q. Zhang, Q. Zhang, J. Wang, S. Zhang and S. Li, *Polymer*, 2010, **51**, 5407-5416.
38 Z. Liu, X. Li, K. Shen, P. Feng, Y. Zhang, X. Xu, W. Hu, Z. Jiang, B. Liu and M.D. Guiver, *J. Mater. Chem. A*, 2013, **1**, 6481-6488.
39 A. Jasti and V.K. Shahi, *J. Mater. Chem. A*, 2013, **1**, 6134-6137.
40 M. A. Hossain, Y. Lim, S. Lee, H. Jang, S. Choi, Y. Jeon, J. Lim and W.G. Kim, *Int. J. Hydrogen Energy*, 2014, **39**, 2731-2739.
41 Z. Zhao, J. Wang, S. Li and S. Zhang, *J. Power Sources*, 2011, **196**, 4445-4450.
42 A. H. N. Rao, S. Y. Nam and T. H. Kim, *J. Mater. Chem. A*, 2015, **3**, 8571-8580.
43 B. Qiu, B. Lin, L. Qiu and F. Yan, *J. Mater. Chem.*, 2012, **22**, 1040-1045.
44 S. Chempath, B. R. Einsla, L. R. Pratt, C. S. Macomber, J. M. Boncella, J. A. Rau and B. S. Pivovar, *J. Phys. Chem. C*, 2008, **112**, 3179-3182.
45 M. Tomoi, K. Yamaguchi, R. Ando, Y. Kantake, Y. Aosaki and H. Kubota, *J. Appl. Polym. Sci.*, 1997, **64**, 1161-1167.
46 J. Wang, S. Gu, R. B. Kaspar, B. Zhang and Y. Yan, *ChemSusChem*, 2013, **6**, 2079-2082.
47 S. C. Price, K. S. Williams and F. L. Beyer, *ACS Macro Lett.*, 2014, **3**, 160-165.
48 O. I. Deavin, S. Murphy, A. L. Ong, S. D. Poynton, R. Zeng, H. Herman and J. R. Varcoe, *Energy Environ. Sci.*, 2012, **5**, 8584-8597.
49 O. M. Page, S. D. Poynton, S. Murphy, A. L. Ong, D. M. Hillman, C. A. Hancock, M. G. Hale, D. C. Apperley and J. R. Varcoe, *RSC Adv.*, 2013, **3**, 579-587.
50 Y. Yang, J. Wang, J. Zheng, S. Li and S. Zhang, *J. Membr. Sci.*, 2014, **467**, 48-55.
51 K. M. Hugar, H. A. Kostalik, and G. W. Coates, *J. Am. Chem. Soc.*, 2015, **137**, 8730-8737.